JOURNAL OF PROPULSION AND POWER
Vol. 25, No. 2, March–April 2009

Effect of Bulk Density on Reaction Propagation in Nanothermites and Micron Thermites

Michelle L. Pantoya*
Texas Tech University, Lubbock, Texas 79409
Valery I. Levitas
Iowa State University, Ames, Iowa 50011
John J. Granier
Texas Tech University, Lubbock, Texas 79409
and
Jack B. Henderson
Netzsch Instruments, Inc., Estes Park, Colorado 80517

DOI: 10.2514/1.36436

The thermite reaction of nanoscale aluminum and molybdenum trioxide particles has revealed a paradoxical relationship between Al particle size and mixture bulk density. Specifically, with micron-scale Al particles, the thermite demonstrates an expected growth in flame speed with increased density, but nanoscale-Al-particle mixtures exhibit an opposing trend. This paper presents new experimental measurements of the thermal properties of this thermite as a function of Al particle size and applies a new oxidation mechanism in an effort to explain the paradoxical results between Al particle size and mixture bulk density. Results show that the nanocomposite's behavior is consistent with a new melt-dispersion oxidation mechanism and convective mode of flame propagation. Compaction-induced damage of the oxide shell and distortion of the shape of spherical particles, as well as reduced free space around Al nanoparticles suppress the melt-dispersion mechanism and reduce flame speed. An additional mode of energy transfer is proposed that is associated with molten Al clusters from the melt-dispersion mechanism that advance faster than the flame velocity. Micron-scale particle reactions may be governed by diffusion such that increased bulk density coincides with increased thermal properties and increased flame speeds.

Introduction

REACTIVE materials are a class of energetic materials that include two or more nonexplosive solids and can include thermites, intermetallics, and metal–polymer mixtures. In application, these materials are often pressed into high-density composites and used as a means for transferring energy to a target material. For this reason, understanding the dynamics of flame propagation for high-density mixtures such as aluminum and a metal oxide is fundamentally important.

Recently, Pantoya and Granier [1] obtained a paradoxical experimental result for unconfined burning of Al + MoO_3 thermites. They showed that whereas flame speed increases with increasing density for micron-particle thermites (as expected), it decreases for nanoparticle thermites (Fig. 1). This result may be best explained using an alternative oxidation mechanism based on melt dispersion rather than diffusion. A curve fit to the data shown in Fig. 1 is $V = A_1 \exp(-2.5\rho)$ for nanoparticle composites (i.e., nanocomposites) and is $V = A_2 \exp(2.0\rho)$ for a micron-particle composites (i.e., micron composites), where flame speed V is in m/s, density ρ is in g/cm^3, and A_1 and A_2 are constant coefficients equal to 602 and 0.1, respectively. Figure 1 indicates that nanocomposites exhibit an exponential decrease in flame speed on the order of a −2.5 exponent with respect to sample density and that micron composites exhibit an exponential increase in flame speed on the order of a 2.0 exponent with respect to sample density [1]. Data were obtained from pellets that were laser-ignited in an ambient environment, and flame-propagation speeds were measured with a high-speed camera.

The goal of this paper is to resolve the paradoxical results found in [1]. One objective of this study is to perform experiments that will resolve the variation in thermal properties such as conductivity and diffusivity as a function of density and Al particle size. Another objective is to apply a mechanochemical theory describing a melt-dispersion mechanism in an effort to explain the paradoxical results found in [1].

Experimental

Because thermal conduction is one of the energy transfer modes for flame propagation, one objective is to determine the influence of densification on the thermophysical properties of micron-vs-nanoparticle thermites. Experiments were designed and conducted using a Netzsch LFA 447 (Laser Flash Analyzer) to determine the thermal diffusivity, specific heat, and thermal conductivity of micron and nanoparticle thermites as a function of density (or porosity).

Passivated 80 nm aluminum powder was provided by NovaCentrix (Austin, Texas). The micron Al used for this study had a 3–4 μm particle diameter and was purchased from Alfa Aesar. Both Al particles are spherical in shape. Separately, each Al powder was mixed with MoO_3 powder provided by Climax (Phoenix, Arizona). The MoO_3 consists of rectangular particles with thicknesses on the order of 5–10 nm and lengths varying from 0.5–1 μm. Micrographs of these individual reactants and mixtures can be seen in [2]. An equivalence ratio ϕ of 1.2 was used and selected based on previous work that showed the highest ignition sensitivity and flame speed for this equivalence ratio of Al + MoO_3 [2,3]. The equivalence ratio was calculated from Eqs. (1) and (2) and based on the following stoichiometric reaction:

$$2Al + MoO_3 \rightarrow Al_2O_3 + Mo$$

In Eqs. (1) and (2) F represents the fuel mass (i.e., Al), O is the oxidizer mass (i.e., MoO_3), MW is the molecular weight, and the subscripts a and st represent actual and stoichiometric:

Received 2 January 2008; accepted for publication 21 September 2008.

*Mechanical Engineering Department; michelle.pantoya@ttu.edu.

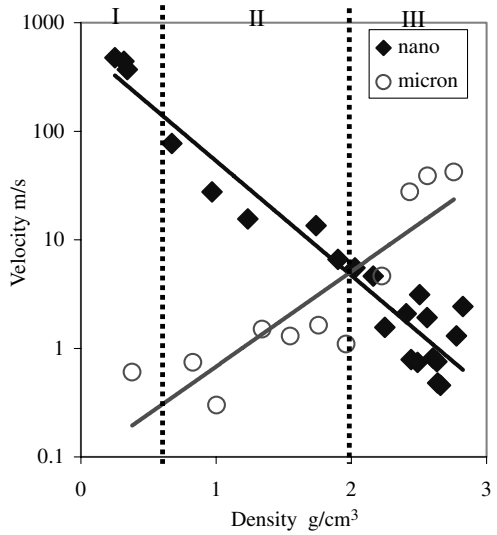

a)

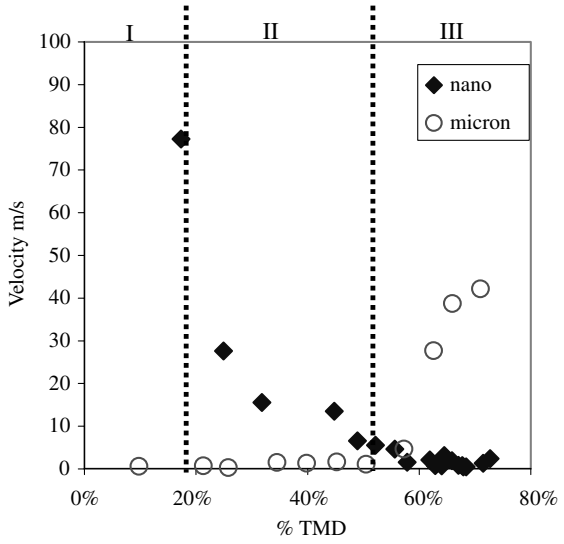

b)

Fig. 1 Flame speed as a function of density (and TMD) for nano- or micron Al particles mixed with nanoscale MoO_3 particles in a) logarithmic and b) normal scales. Experimental data are from Fig. 9 in [1]. Note Fig. 1b is provided to illustrate the relatively week dependence of flame velocity on density in the range 20–60% TMD.

$$\phi = \frac{F/O_a}{F/O_{\text{st}}} \tag{1}$$

where

$$\frac{F}{O_{\text{st}}} = \frac{2(\text{MW}_{\text{Al}})}{\text{MW}_{\text{MoO}_3}} \tag{2}$$

Based on the preceding reaction and Eq. (2), $F/O|_{\text{st}}$ is 0.5625. It should also be noted that Al is passivated with an Al_2O_3 coating. For the 80 nm Al powder, the active Al concentration Y is 80.4% and remains unchanged throughout experimentation. This value was provided by the supplier and used to determine mass ratios of fuel and oxidizer powders. The mass percentage of Al powder (Al with oxide coating) is determined by

$$X = \frac{\phi \cdot F/O_{\text{st}}}{Y + (\phi \cdot F/O_{\text{st}})} \tag{3}$$

Passivated nanometer (nano) Al powder was mixed at a mass ratio of 45.6% (X) with 54.4% ($1 - X$) MoO_3. The micron Al used for this study has an active Al concentration of 98%. This led to a micron Al mass ratio of 40.8% Al to 59.2% nm MoO_3.

The dry-powder mixtures of Al and MoO_3 were suspended in hexanes at a ratio of 1 g powder to 40 ml of solvent. Mixing was achieved by sonication such that agglomerates were reduced as confirmed via scanning electron microscopy (SEM) images in [2]. A 1-cm-diam sonic probe (Misonix 3000) was submerged approximately 3 cm below the liquid level of 60 ml (1.5 g of powder) and actively sonicated for 60 s by an alternating duty cycle of 10 s on/off intervals at a power of 42 W. The wet solution was then dried on a 40°C hot plate in a Teflon-coated steel pan under a fume hood. After allowing the hexanes to evaporate for 12 min, a dry fine powder settled to the bottom of the pan. The dry mixture was reclaimed using a conductive brush (Thunderon 22 bristle, Gordon Brush) grounded to the pan. This loose powder sample was stored under standard-grade argon and controlled humidity until it was pressed into cylindrical pellets within 24 h from the mixture preparation.

Loose powders were pressed into compact cylindrical pellets using a three-piece die, as shown in Fig. 2a, with a 50 t manual hydraulic press (Carver, Inc.). A schematic of the pressure die is shown in Fig. 2b. A prespecified mass of powder thermite mixture was initially loaded into the top orifice of the barrel with the base plunger forming a seal at the base orifice of the barrel. The top plunger was then hand-aligned into the top orifice of the barrel and the entire assembly was loaded in the hydraulic press. A compression load was applied to the entire assembly until one of two critical stages was met:

1) With load pressing, the entire assembly is compression-loaded until a desired pressure is achieved, as indicated by a hydraulic-pressure gauge on the Carver press.

2) With shim pressing, the pellet length is precalculated to achieve a specific density based on the input powder mass. This pellet length is guaranteed by placing a series of metal shims between the top plunger head and the top surface of the barrel.

After each pellet was formed under compression, the bottom plunger was removed (if used, the shims were also taken out) and the entire assembly was flipped vertically. A holed spacer was then placed on the now-top surface of the barrel and the sample pellet was extruded

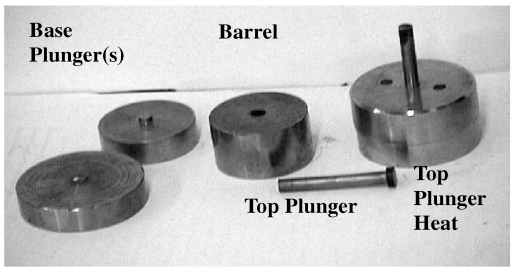

a)

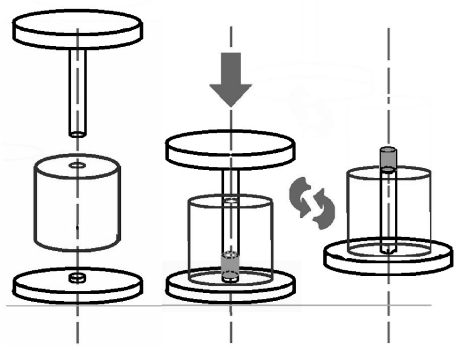

b)

Fig. 2 Cylindrical pressure die: a) top plungers M2 tool steel (McMaster-Carr) (diameter is 6.52 mm, length is 3.5 cm, barrel 316 stainless steel and 1018 steel are used, inside diameter is 0.477 mm, length is 3 cm, short-base 316 stainless steel, length is less than 2.54 mm) and b) schematic of the three-step procedure for the compression die assembly.

into the hole of the spacer. The bulk density of the sample was then calculated based on measured dimensions and actual pellet mass.

For the laser flash analyzer (LFA) experiments, four compressed wafers were prepared using a 12.7 mm die with specified shims to create the prescribed sample length. The samples were prepared with a 12.7 mm diameter by 2 mm length. Because the sample volume was well defined, the powder mass was varied during pressing to generate a range of sample densities to perform LFA experiments on various-density nano- and micron composites. A minimum practical density was observed due to the rigidity of the samples for handling (i.e., if the sample was too soft, it would crumble and break during handling and mounting). A maximum-achievable density was observed due to sample quality (some high-density samples would stratify and crack into thin layers) and failure limitations of the die. The minimum- and maximum-achievable pellet densities are uniquely determined by the composite powder (and Al particle size). A common approach for describing bulk density is in terms of a theoretical maximum density (TMD) defined as the ratio of measured bulk density based on sample mass and volume divided by the density calculated based on the weighted average of the densities of each reactant in the mixture. A density range from 1.07 to 1.79 g/cm^3 (27.6 to 46% TMD) was generated for nanocomposites. A slightly overlapping density range of 1.54 to 2.52 g/cm^3 (39.7 to 64.7% TMD) was generated for the micron composites.

The LFA uses a xenon flash lamp to fire an energy pulse at one side of a thin wafer sample, and an infrared detector measures the temperature of the opposite side of the wafer. The specific heat c_p is measured by comparing the sample temperature to a reference sample of known specific heat. The thermal diffusivity α is measured by the transient temperature response of the material. The LFA 447/2 allows the user to heat the sample with a furnace to make thermal property measurements from ambient temperatures to 300°C. Each sample was cycled through two heating programs from 25 to 300°C and the conductivity, specific heat, and diffusivity were measured at 25°C increments. Once c_p, α, and density ρ are known, the thermal conductivity λ can be backcalculated by $\lambda = \alpha \rho c_p$.

Results

Figure 3 shows the temperature- and bulk-density-dependent thermal diffusivity and thermal conductivity for both the nano- and micron composites. Figure 3 shows an increasing trend for both diffusivity and conductivity with bulk density. The overlap of the curves two high-density nanocomposites and two low-density micron composites suggests that the diffusivity and conductivity are independent of Al particle size and Al_2O_3 concentration. These results suggest that high-density thermites will provide improved thermal transport by conduction, compared with low-density thermites. This is consistent with the increase in flame speeds in micron composites shown in Fig. 1. The higher-density micron composites transport heat away from the flame zone more effectively, allowing faster heating of nearby reactants and less resistance to flame propagation. However, trends in thermal properties are opposite to the trends in flame speed for nanoparticle thermites.

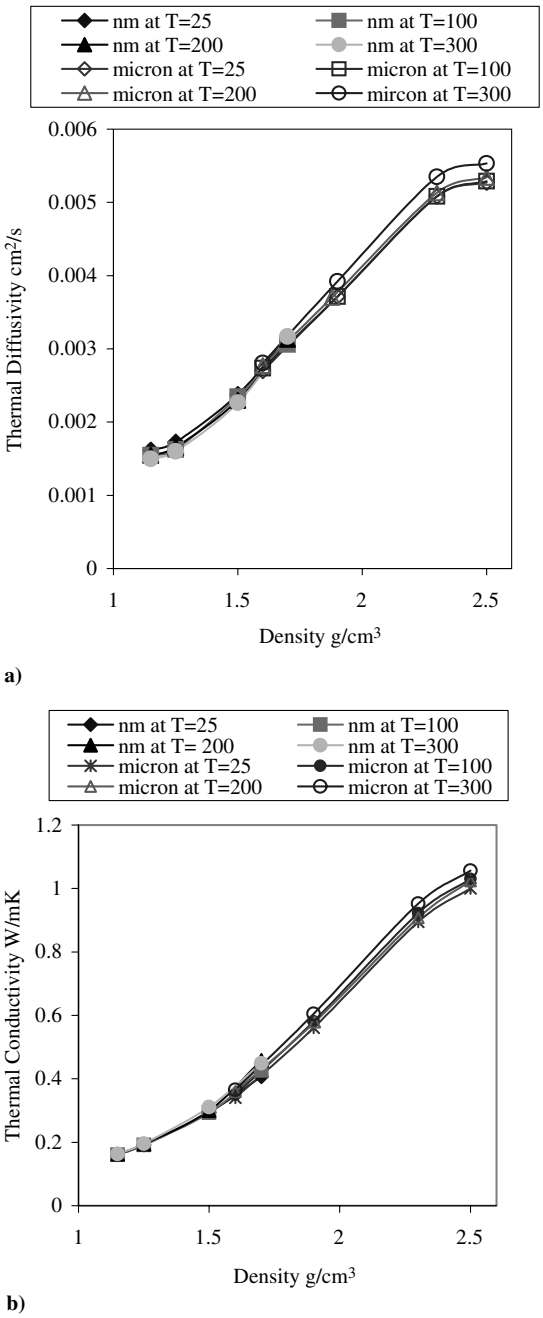

Fig. 3 Thermal properties for the nano- and micron composites of Al and MoO_3: a) thermal diffusivity and b) thermal conductivity.

Discussion

Effect of Compaction on the Flame Velocity for Micron Composites

The electron microscopy images in Fig. 4 show that the MoO_3 fractures during compaction. It is also expected that ductile aluminum deforms plastically, reducing void volume, whereas the brittle alumina oxide shell is damaged. For micron particles, the oxidation mechanism is related to diffusion of oxygen or aluminum through the oxide shell. Pressing micron particles increases the flame speed because the following occurs in the pressing process:

1) The oxide shell is damaged, providing easier diffusion paths for oxygen and/or Al and accelerating the oxidation reaction.

2) The contact area is increased between the Al particles and MoO_3, thus reducing the diffusion path.

3) The thermal conductivity and thermal diffusivity of the composite increase, leading to faster heat transfer according to conductive flame-propagation modes.

Thus, the density dependence on the flame speed for micron composites is consistent with the diffusive oxidation mechanism and conductive flame-propagation mode.

Melt-Dispersion Mechanism for Nanocomposites

Theories describing Al oxidation are based on diffusion of an oxidizer to the Al-fuel-particle core or Al toward the oxidizer through a growing aluminum oxide shell surrounding the Al particle [4]. However, studies on nanoscale-Al-particle reactions have shown that when the Al particle radius reduces to the nanoscale (in contrast to traditional 1–100 μm size), reaction rates drastically increase. For example, flame-propagation speeds are reported to reach 1 km/s for loose $Al + MoO_3$ and $Al + Fe_2O_3$ nanoparticulate mixtures in contrast to 1 cm/s for micron-size Al particles [2,5], and ignition delay times are reduced by up to 3 orders of magnitude [3]. Diffusion through an oxide shell does not appear to apply for nano-Al combustion. For example, the characteristic reaction time (approximately estimated as pressure rise time) observed in

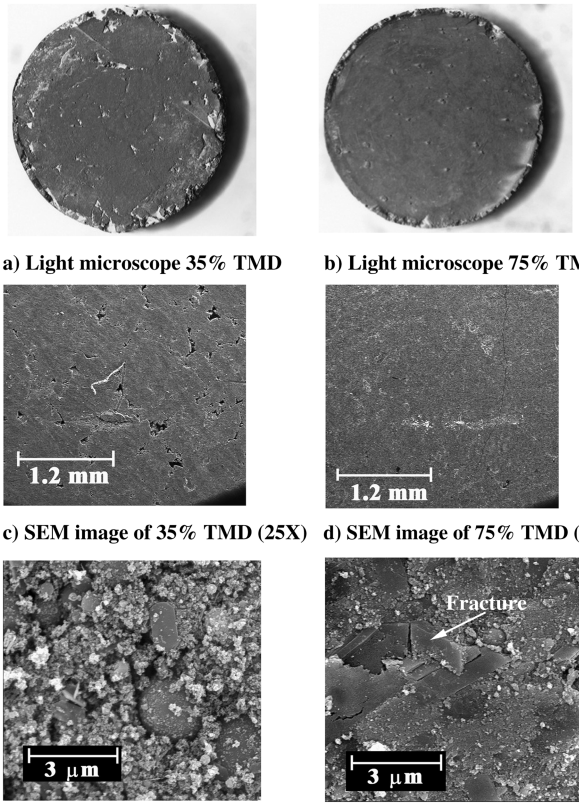

a) Light microscope 35% TMD b) Light microscope 75% TMD

c) SEM image of 35% TMD (25X) d) SEM image of 75% TMD (25X)

e) SEM image of 35% TMD (15kX) f) SEM image of 75% TMD (15kX)

Fig. 4 Light microscope and SEM images of micron Al and MoO_3 compressed samples. The images in the left column are different magnifications of a 35% TMD (1.36 g/cm^3) and the right-column images are 75% TMD (2.92 g/cm^3).

flame-propagation experiments is 10 μs [2,5]. For slow heating, when the melt-dispersion mechanism cannot be activated and oxidation occurs via the diffusion of oxygen and Al through the oxide shell, oxidation is far from complete, even after 1 s [6].

Recently, a mechanochemical mechanism describing nanoparticle-Al reactions has been suggested for fast oxidation [7,8]. The theory explains that fast heating (10^6 to 10^8 K/s) creates huge internal thermal stresses due to the difference in thermal expansion coefficients between Al and Al_2O_3 and volumetric strain during Al melting. Because of the small size of the amorphous oxide shell (shell thickness δ of roughly 1–4 nm), it is almost defect-free and the shell strength approaches the theoretical strength.

For small particles (ratio of particle radius to shell thickness $R/\delta < 19$), the oxide shell can fracture after complete melting of the Al core. This mechanism is described in detail in [7–9] and will be summarized here. Aluminum melting is accompanied by a volume increase of 6%, and pressure within the molten core becomes high (0.1–4 GPa). This magnitude of pressure buildup could lead to dynamic spallation of the oxide shell, which would result in the complete exposure of the liquid-Al droplet with unbalanced pressure between the exposed Al surface and the internal Al droplet. The unbalanced pressure leads to an unloading wave within the liquid-Al droplet and creates a tensile pressure of the same order of magnitude. The tensile pressure disperses the Al droplet into small clusters that fly with a high flame speed (100–250 m/s), the oxidation of which is not limited by diffusion [7].

For large (micron-scale) particles, the shell has been shown to fracture before the Al melts, and so the pressure in the Al core is low (10 MPa) and an unloading wave cannot disperse the solid Al [7–10]. As the reaction proceeds, the bare Al core is quickly covered by a defective oxide film, which continues to grow in thickness. There is some acceleration of oxidation during the fracture, followed by healing and traditional diffusion-controlled mechanisms for further oxidation through the defective shell.

Currently, there is no direct experimental confirmation of the melt-dispersion mechanism. However, there are quite plausible theoretical justifications in [7], and this is the only known mechanism that allows resolution of basic puzzles in nanothermite combustion that cannot be explained by the diffusion mechanism:

1) The reactivity of nanothermites (high flame velocity and small ignition time delay) is extremely high.

2) The particle reactivity (evaluated as flame velocity and ignition time delay) of the ratio $M = R/\delta$ (particle size over oxide thickness) is independent below some critical ratio $M_c = 19$.

3) Nanoflakes that react significantly slower than nanosized spherical particles [11] have low reactivity.

4) The nanoparticle reactivity with damage of the oxide shell (which will be also elaborated in the current paper) is suppressed.

Recently, two additional experimental results supporting the melt-dispersion mechanism and contradicting the diffusion mechanism have been reported:

1) The flame rate is determined by the ratio of the Al core radius to shell thickness $M = R/\delta$ and is independent of R and δ separately [9,12]. This result was found both for nanoparticles [9] and for 1–3 μm particles [12].

2) After heating of Al nanoparticles to $T = 1100$°C, at a heating rate of $\sim 10^3$ K/s (when the diffusion mechanism was proven), the burn time exceeds 1 s [10]. After fast heating of $\sim 10^7$ K/s (when the melt-dispersion mechanism can be activated), the burn time was only 500 μs [13,14].

The following discussion assumes validity of the melt-dispersion mechanism and readers are referred to [7–9] for further details on this theory. We will apply this mechanism and interpret the effect of compaction of aluminum nanoparticles on the flame speed.

Effect of Compaction on the Flame Velocity for Nanoparticle Thermites

Pressing powders in a die damages the oxide shell of both nano- and micron Al particles [1]. The exposed Al surface will be covered by an oxide shell; however, damaged sites remain. Increasing the pressure applied to the particles results in increased density and an increase in the damage to the oxide shell. Local pressure at the contact between two Al particles or an Al and oxidizer particle is much higher than the average pressure, because the actual contact area is much smaller than the nominal area (area of the largest cross section of a sphere) $\pi d^2/4$. Damage of the oxide shell should suppress the melt-dispersion mechanism for the following reasons:

1) Defects reduce the strength of alumina by orders of magnitude (from the theoretical strength to the strength of a bulk sample with defects) and consequently reduce the pressure inside the molten aluminum, which drastically reduces the probability of cavitation and melt dispersion.

2) Imperfections cause localized fracture near the defect (similar to the fracture of micron-size particles or nanoparticles at slow heating) and flow of the molten Al through the holes, rather than homogeneous fracture and spallation of the entire oxide shell. The pressure in the particle drops to zero when less than 10% of the molten Al flows out.

3) Pressing may distort the spherical particle geometry, which reduces the chances of simultaneous fracture of the entire shell and leads to localized fracture.

4) The melt-dispersion mechanism can operate if there is enough free space around Al particles. An increase in bulk density above some critical value reduces the void volume, leaving less space for the flight of liquid-Al clusters, rendering the melt-dispersion mechanism less effective. If, however, fracture and spallation of the oxide shell are delayed above the temperature when MoO_3 begins sublimation (above 973 K), then additional space appears for the melt dispersion.

5) Some mass of Al reacts during the healing of the damaged sites, leaving less Al to react in a flame. Because the nanoparticle area-to-volume ratio is much larger, this Al loss is much more pronounced for nanocomposites than for a micron-scale thermites. However, for loose powder, this factor is ruled out by our recent experiments [9],

which were performed with loose powder using Al particles with different oxide-shell thicknesses. Results show that an increase in the thickness of the oxide shell by a factor of 2 (from 1 to 2 nm for particles 50 nm in diameter and 2 to 4 nm for particles 120 nm in diameter), which leads to a decrease in Al content by approximately 10%, did not reduce the flame speed.

Thus, one of the main reasons for the reduction in flame speed with the increase in sample density for nanocomposites is the damage of the oxide shell and distortion of the particles that reduce the number of particles that react according to the melt-dispersion mechanism.

It was experimentally shown that grinding Al particles causes damage to the oxide shell and leads to 2-times-slower flame velocities, even without changing the density of the composite [8]. On the other hand, vibrational compaction should not damage the oxide shell and suppress the melt-dispersion mechanism. Indeed, vibrational change in density in the range of 5–10% of TMD did not change the flame-propagation rate significantly [2].

Flame-Propagation Mode

Convection and thermal conduction can be considered to be the main modes for energy propagation. For loose powders, convection is the main mode of flame propagation, which may be enhanced above 973 K when MoO_3 starts to sublimate. An increase in the nanocomposite density above a critical value reduces the number of connected channels. The increase in composite density will increase the resistance to gas flow, suppressing convection but increasing thermal diffusivity. The result that micron-composite flame speeds increase with increased density suggests the following. The contribution to the flame speed due to convection (that is dominant at low densities) is suppressed more slowly with the growth in density than with the contribution from thermal conduction that is promoted. For high densities, thermal conduction is dominant and convection does not play a significant role for both micron and nanocomposites. The thermal diffusivity of the micron and nanocomposites range from 0.0015 to 0.005 cm^2/s, with increased density such that the reduced flame speed for nanocomposites compared with micron composites for larger than 65% TMD cannot be related to the thermal properties of the mixture.

For up to 55% TMD, some nanoparticles that have not been substantially deformed may react according to the melt-dispersion mechanism. Indeed, compaction pressures for nanocomposites start to drastically grow above 55–60% TMD [1], which intensifies the damage to the oxide shell of most Al particles. Also, flame speeds on the order of several meters/second may not provide a sufficiently high heating rate for the operation of the melt-dispersion mechanism for densities larger than 60% TMD. Indeed, for nano- and micron Al of varying proportions combined with MoO_3, a sharp increase in flame speed is observed for pellets with ~50% nano- and micron particles, and distribution also corresponds with flame speeds from 5 to 10 m/s [15]. This sharp increase may be related to activation of the melt-dispersion mechanism in nanoparticles. Higher temperatures may lead to a more complete reaction of micron particles that also contributes to the higher flame speed. The flame speed of 5 to 10 m/s corresponds to 55–60% of TMD in Fig. 1, which is consistent with estimates for the upper bound of bulk density for the melt-dispersion mechanism. The heating rate corresponding to the activation of the melt-dispersion mechanism can also be estimated from experimental data. For the flame rate of 1 km/s in [8], the heating rate of 10^8 K/s was estimated as 1000 K/10 μs, because temperature in a reaction zone grows by ~1000 K within ~10 μs. For the same width of the reaction zone, the heating rate is proportional to flame speed. Thus, for the flame speed of 10 m/s, the heating rate can be estimated as 10^6 K/s.

Velocities of dispersed liquid clusters may reach and exceed 100 m/s [7–9], which is higher than the flame speed for densities greater than 20% TMD. These dispersed liquid clusters can serve as an additional mode of energy transfer by effectively preheating unreacted particles ahead of the flame front (see Fig. 5). In fact, the relatively weak dependence of the flame velocity for nano Al with increasing density for the densities in the range of 20 to 55% TMD (see Fig. 1b) may be a signature of the contribution of this flame-propagation mode.

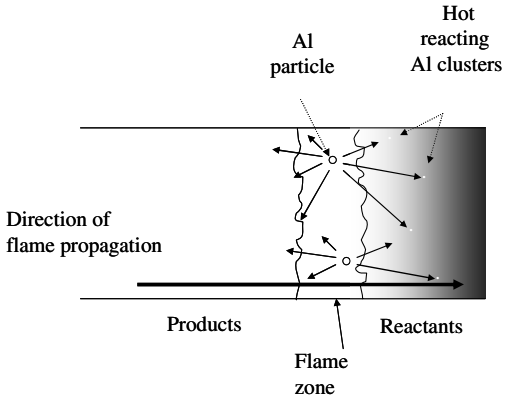

Fig. 5 Schematic diagram illustrating that nanoparticles react via a melt-dispersion mechanism. Initially, melting of Al creates huge internal pressures followed by spallation of the oxide shell, exposing the molten core and generating an unloading pressure wave that disperses small Al clusters.

Flame Speed at Densities Larger than 65% TMD

Surprisingly, for mass densities exceeding 65% TMD, the flame speed for micron composites is significantly larger than for nanocomposites. If the melt-dispersion mechanism cannot operate for such densities, the classical diffusion mechanism can be applied for both particle sizes. The thermal diffusivity of both types of particles is practically the same, and so the flame-propagation mode cannot explain this difference.

The main reason for such unexpected behavior can be explained with the help of Fig. 6. The MoO_3 has a sheetlike shape, whereas Al particles are spherical. After large deformation of soft Al micron-scale particles, the contact area between the Al particles and oxidizer increases drastically. For nanoparticles, the contact area between the Al and MoO_3 increases for the first layer of Al particles only. More important, multiple oxide shells for nanoparticle agglomerates create multiple diffusion barriers, in comparison with a single oxide shell for a micron-scale particles. Flow of the molten Al is not as effective for high-density pellets. Thus, the main mechanism that causes reduced flame speeds for nanoparticles is related to slower diffusion. This may be prevented to some extent by using spherical oxidizer particles.

Another possible contribution to this phenomenon is related to the lower active Al content in nanoparticles than with micron particles, both due to the presence of an initial oxide shell and potentially higher oxidation during the healing of damaged particles. Thus, for 80-nm-diam particles, the initial active Al content was 80%, in comparison with 97–99% of Al content for micron particles. This difference did not play a major role for loose powder [15]. However, the active Al content may be important for high densities, when

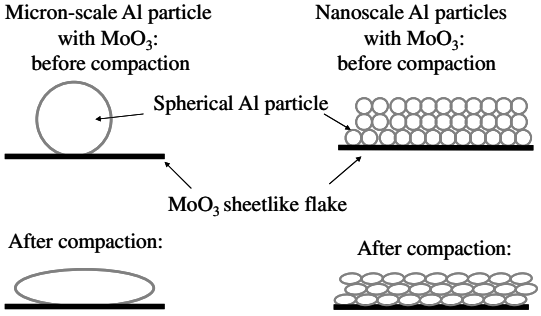

Fig. 6 Schematic geometry of compaction of micron and nanoscale spherical particles with a MoO_3 sheetlike flake. After large deformation of soft Al particles, multiple oxide shells for a nanoparticle conglomerate create multiple diffusion barriers, in comparison with a single oxide shell for a micron-scale particle.

diffusion for nanoparticles is slower than for micron particles, perhaps due to geometric reasons.

Conclusions

The opposing trends in flame speed versus bulk density that were observed for micron and nanocomposites are intriguing and nontrivial. Nanocomposites exhibit a decrease in flame speed as the composite is pressed to higher densities. This paper supplemented these previously published results with new experiments measuring the thermal properties of conductivity and diffusivity for $Al + MoO_3$ composites as a function of Al particle size, bulk density, and temperature. Additionally, the melt-dispersion mechanism recently proposed for nano-Al-particle combustion has been applied toward interpreting the unique relationship between mixture density and flame speed for nanocomposites.

Results indicate that thermal properties such as thermal diffusivity and conductivity do not significantly vary for nanocomposites compared with micron composites and thermal diffusivity ranges from 0.0015 to 0.005 cm^2/s. The behavior of micron composites versus bulk density is consistent with the diffusive oxidation mechanism. Compaction-induced damage of the oxide shell and increased contact area between Al and the oxidizer promotes the diffusion mechanism and suppresses convection, whereas increased thermal diffusivity intensifies the conductive flame-propagation mode. The behavior of nanocomposites can be explained using the melt-dispersion oxidation mechanism [7,8] for densities below 55 % TMD. Thus, damage of the oxide shell and distortion of the shape of spherical particles during compaction, as well as reduced free space around Al nanoparticles, suppress the melt-dispersion mechanism and reduce the propagation rate. The melt-dispersion mechanism may be operative for heating rates above 10^6 K/s, which corresponds to flame speeds above 5 to 10 m/s. The lower flame speed of nanocomposites compared with micron composites for densities above 65% TMD can be related to multiple barriers to diffusion, due to the multiple oxide shells along the diffusion path from a sheet-shaped oxidizer (see Fig. 6). Another reason may be associated with the lower Al and larger alumina contents, both due to initial oxide-shell thickness and more intense oxidation of Al nanoparticles during shell healing after compaction.

Approximate interpretation for the curve for nano Al in Fig. 1 can be summarized as follows. In regions I and II, a decrease in the flame velocity is due to suppression of the melt-dispersion mechanism. In region II, the melt-dispersion mechanism also induces a mode of energy transfer and heating ahead of the flame front when the hot reacting liquid-Al clusters fly at the velocity that exceeds the flame velocity. In region III, flame velocity for nanocomposites is smaller than for micron composites because of multiple barriers to diffusion due to multiple oxide shells along the diffusion path from a sheet-shaped oxidizer. For micron particles, significant growth in flame velocity occurs above 60% TMD and is due to an increase in contact area and promotion of diffusion.

The flame speed of high-density thermites may be increased by avoiding the suppression of the melt-dispersion mechanism. One can attempt pressing while reducing the loading force on individual particles, such that the shell may not be damaged during the pressing process. This could be investigated by combining pristine nanoparticles with a liquid Teflon binder and mold-casting the pellet. This technique is used by manufacturers of reactive materials (such RM-4 by GSI). Other soft reactants such as ductile metals can be used as well. Also, the flame speed can be increased for higher densities in which the melt-dispersion mechanism cannot be activated by substituting flake-shaped oxidizers with spherical nanoparticles of a size comparable with the Al nanoparticles.

Acknowledgments

The authors gratefully acknowledge support from the Office of Naval Research, under contract numbers N000140710318 and N000140810104, and our program managers, Judah Goldwasser and Clifford Bedford. The National Science Foundation is also acknowledged under contract number CBET-0755236. M. Pantoya acknowledges support by the U.S. Army Research Office, contract number W911NF-04-1-0217, and Ralph Anthenien. Additional gratitude is acknowledged to Kurt Schroder from NovaCentrix, Corporation for his helpful discussions and donations of research quantities of powder materials.

References

[1] Pantoya, M. L., and Granier, J. J., "Combustion Behaviors of Highly Energetic Thermites: Nano Versus Micron Composites," *Propellants, Explosives, Pyrotechnics*, Vol. 30, No. 1, 2005, pp. 53–62. doi:10.1002/prep.200400085

[2] Bockmon, B., Pantoya, M. L., Son, S. F., Asay, B. W., and Mang, J., "Combustion Velocities and Propagation Mechanisms of Meta-Stable Intermolecular Composites," *Journal of Applied Physics*, Vol. 98, No. 6, 2005, pp. 064–903. doi:10.1063/1.2058175

[3] Granier, J. J., and Pantoya, M. L., "Laser Ignition of Nanocomposite Thermites," *Combustion and Flame*, Vol. 138, No. 4, 2004, pp. 373–383. doi:10.1016/j.combustflame.2004.05.006

[4] Trunov, M. A., Mirko, S., Xiaoying, Z., and Dreizin, E. L., "Effect of Polymorphic Phase Transformations in Al_2O_3 Film on Oxidation Kinetics of Aluminum Powders," *Combustion and Flame*, Vol. 140, No. 4, 2005, pp. 310–318. doi:10.1016/j.combustflame.2004.10.010

[5] Plantier, K. B., Pantoya, M. L., and Gash, A. E., "Combustion Wave Speeds of Nanocomposite Al/Fe_2O_3: The Effects of Fe_2O_3 Particle Synthesis Technique," *Combustion and Flame*, Vol. 140, No. 4, 2005, pp. 299–309. doi:10.1016/j.combustflame.2004.10.009

[6] Park, K., Lee, D., Rai, A., Mukherjee, D., Zachariah, M. R., "Size Resolved Kinetic Measurements of Aluminum Nanoparticle Oxidation with Single Particle Mass Spectrometry," *Journal of Physical Chemistry B*, Vol. 109, No. 15, 2005, pp. 7290–7299. doi:10.1021/jp048041v

[7] Levitas, V. I., Asay, B. W., Son, S. F., and Pantoya, M. L., "Melt Dispersion Mechanism for Fast Reaction of Nanothermites," *Applied Physics Letters*, Vol. 89, No. 7, 2006, pp. 071–909. doi:10.1063/1.2335362

[8] Levitas, V. I., Asay, B. W., Son, S. F., and Pantoya, M. L., "Mechanochemical Mechanism for Fast Reaction of Metastable Intermolecular Composites Based on Dispersion of Liquid Metal," *Journal of Applied Physics*, Vol. 101, No. 8, 2007, Paper 083524. doi:10.1063/1.2720182

[9] Levitas, V. I., Pantoya, M. L., and Dikici, B., "Melt-Dispersion Versus Diffusive Oxidation Mechanism for Aluminum Nanoparticles: Critical Experiments and Controlling Parameters," *Applied Physics Letters*, Vol. 92, 2008, Paper 011921. doi:10.1063/1.2824392

[10] Rai, A., Lee, D., Park, K., and Zachariah, M. R., "Importance of Phase Change of Aluminum in Oxidation of Aluminum Nanoparticles," *Journal of Physical Chemistry B*, Vol. 108, No. 39, 2004, pp. 14793–14795. doi:10.1021/jp0373402

[11] Eapen, B. Z., Hoffmann, V. K., Schoenitz, M., and Dreizin, E. L., "Combustion of Aerosolized Spherical Aluminum Powders and Flakes in Air," *Combustion Science and Technology*, Vol. 176, No. 7, 2004, pp. 1055–1069. doi:10.1080/00102200490426433

[12] Levitas, V. I., Pantoya, M. L., and Watson, K. W., "Melt-Dispersion Mechanism for Fast Reaction of Aluminum Particles: Extension for Micron Scale Particles and Fluorination," *Applied Physics Letters*, Vol. 92, No. 1, 2008, pp. 001–1921. doi:10.1063/1.2824392

[13] Bazyn, T., Krier, H., and Glumac, N., "Combustion of Nano Aluminum at Elevated Pressure and Temperature Behind Reflected Shock Waves," *Combustion and Flame*, Vol. 145, No. 4, 2006, pp. 703–713. doi:10.1016/j.combustflame.2005.12.017

[14] Bazyn, T., Krier, H., and Glumac, N., "Evidence for the Transition from the Diffusion Limit in Aluminum Particle Combustion," *Proceedings of the Combustion Institute*, Vol. 31, Jan. 2007, pp. 2021–2028. doi:10.1016/j.proci.2006.07.161

[15] Moore, K., Pantoya, M. L., and Son, S. F., "Combustion Behaviors Resulting from Bimodal Aluminum Size Distributions in Thermites," *Journal of Propulsion and Power*, Vol. 23, No. 1, 2007, pp. 181–185. doi:10.2514/1.20754

S. Son
Associate Editor